LUNAR IRON AND TITANIUM ABUNDANCE ALGORITHMS BASED ON SELENE (KAGUYA) MULTIBAND IMAGER DATA. H. Otake[1] , M. Ohtake[2] and N. Hirata[3], [1]JAXA Space Exploration Center, Japan Aerospace Exploration Agency, 3-1-1, Yoshinodai, Chuo-ku, Sagamihara, Kanagawa, 252-5210, JAPAN, ootake.hisashi@jaxa.jp, [2]The Institute of Space and Astronautical Science, Japan Aerospace Exploration Agency, [3]The University fo Aizu.

Introduction: The iron and titanium contents of the lunar surface from Clementine spectral reflectance measurements have been derived with a spatial resolution of 200m [1-2].

The Multiband Imager (MI) of the SELENE (KAGUYA) mission was a high-resolution multispectral imaging camera with a spatial resolution of 20m in five visible bands and 62m in four near-infrared bands from the 100km orbit altitude [3]. Small but geologically significant areas such as crater central peaks, crater walls, and ejecta have been investigated utilizing MI's high-spatial resolution and high-quality image data (i.e., high S/N ratio, high MTF, and lossless compression data).

We present algorithms for deriving the abundances of iron and titanium on the lunar surface based on MI image data that have been calibrated [4] and released to the public.

Mapping Iron and Titanium Concentration: Lucey et al. [1] presented trends related to iron content and maturity by plotting the NIR/VIS ratio versus the VIS reflectance for returned lunar samples. An angular parameter was defined by a sample's location in the ratio-reflectance plot. The relationship between the iron content of the samples and the spectral parameter was used to transform the remotely measured spectrum to iron composition.

Lucey et al.[1] also presented a method and the final version of mapping equations for determining the titanium content of lunar materials from Clementine measurements of the 415nm and 750nm reflectance. They defined a titanium-sensitive parameter by performing a coordinate rotation in UV/VIS ratio versus VIS reflectance space. The transformation projects the spectral effects of opaque minerals (ilmenite) onto one axis, and the resulting parameter values were found to correlate well with sample titanium content [1].

Image Data and Sample-Return Locations: Nine bands of digital images from 415nm to 1550nm at 20m/pixel (UV/VIS) and 62m/pixel (NIR) spatial resolution have been produced and released to the public. These images have been radiometrically calibrated and rubber-seated to standard spectral bands, as described in [4] as Level 2B. Additional geometric correction (described in [3] as option 2), photometric normalization (described in METHODS of [5]), and calibration to absolute reflectance using MI62231SaS reflectance and the correction factor in Table 3 in [4] were also applied.

Image cubes containing the six Apollo sample return stations were extracted from the MI image data. The number of sampling stations are 53, especially increased at Apollo 12 and 14 from that for Clementine [1] due to the higher spatial resolution of MI. The number of pixels averaged at each station has also changed: no sampling stations were averaged (i.e., 1 x 1 pixel).

Derivation of Iron and Titanium Abundance Equations: We used the same approach as Lucey et al.[1] (Fig.1) to determine equations for TiO_2 content :

$$\theta_{Ti} = \arctan\{[(R_{415}/R_{750}) - 0.208]/(R_{750} - (-0.108))\}$$

$$wt\%\ TiO2 = 0.72 \times \theta_{Ti}^{14.964}$$

We also used the same approach as Lucey et al.[1] (Fig.2) to determine equations for FeO content:

$$\theta_{Fe} = \arctan\{[(R_{950}/R_{750}) - 1.250]/(R_{750} - (0.037))\}$$

$$wt\%\ FeO = 20.527 \times \theta_{Fe} - 12.266$$

Results: The standard deviation for the fit are 0.43wt% for titanium content and 0.81wt% for iron content which are smaller than the 0.93wt% and 1.29wt% determined with Clementine image data [1].

Figure 3 depicts a global titanium content map, and Fig.4 presents iron content map, using MI image data and the above equations. On a global scale, both titanium and iron contents have similar distributions in MI and Clementine image data: however, meticulous comparison and other methods such as [6-8] will be needed in the future.

References: [1] P.G. Lucey, D.T. Blewett, and B.L. Jolliff (2000) *J. Geophys. Res., 105,* 20,297-20,305. [2] D.J. Lawrence et al. (2002) *J. Geophys. Res., 107,* 13,1-13,26. [3] M. Ohtake et al. (2008) *Earth Planets Space, 60,* 257-264. [4] M. Ohtake et al. (2010) *Space Sci. Review, 154,* 57-77. [5] M. Ohtake et al. (2009) *Nature, 461,* 236-240. [6] B.B. Wilcox, P.G. Lucey, and J.J. Gillis (2005) *J. Geophys. Res., 110,* E11001. [7] D.J. Lawrence et al. (2002) *J. Geophys. Res., 107,* E12, 5130. [8] S.L. Mouelic et al. (2002) *J. Geophys. Res., 107,* 5074.

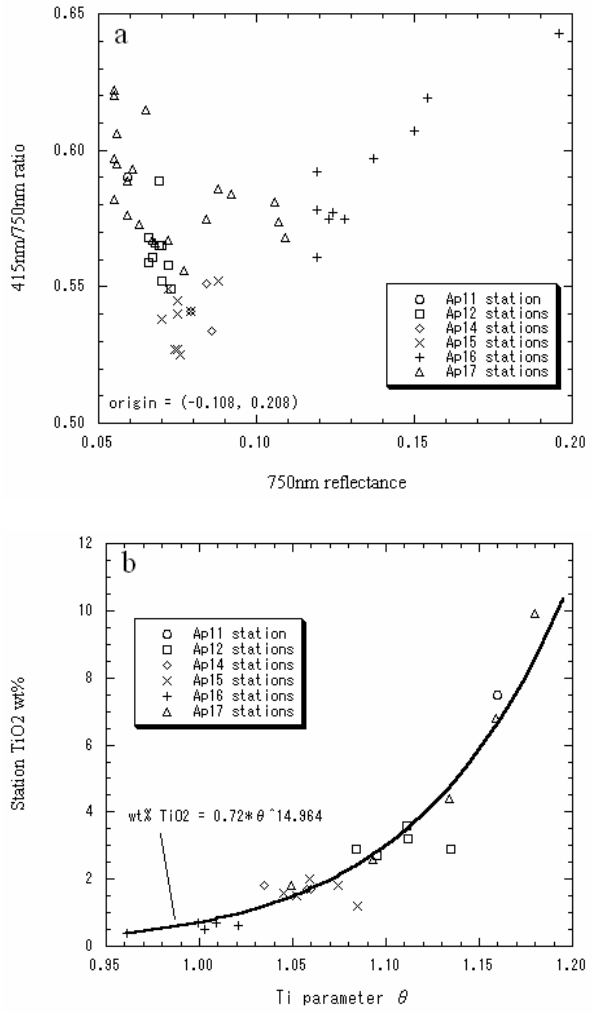

Figure 1. (a) UV-VIS ratio and VIS reflectance plot for sample return sites observed by MI. (b) Plot of TiO_2 content of returned lunar soils and the spectral titanium parameter θ derived from MI data.

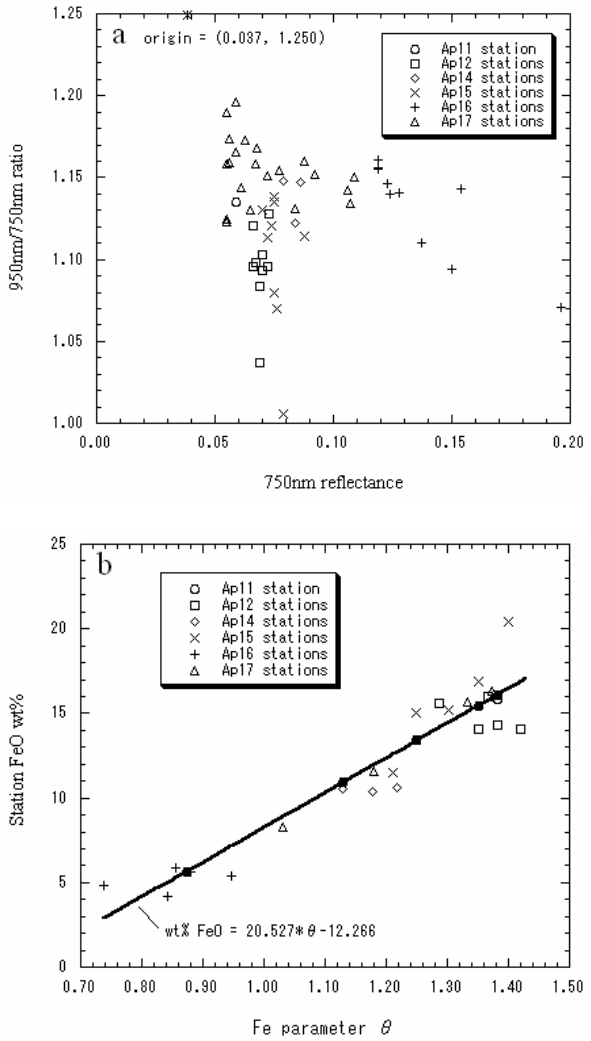

Figure 2. (a) VIS-NIR ratio and VIS reflectance plot for sample return sites observed by MI. (b) Plot of Fe content of returned lunar soils and the spectral iron parameter θ derived from MI data.

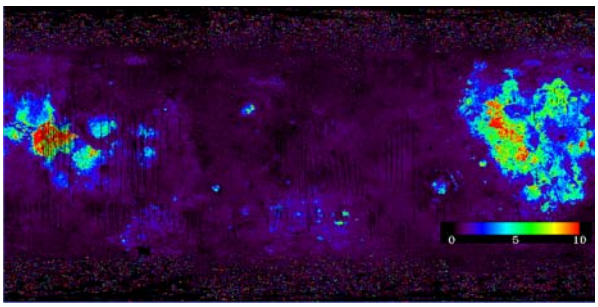

Figure 3. Global titanium content map derived from MI data.

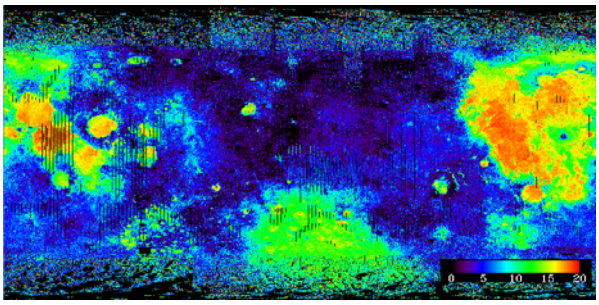

Figure 4. Global iron content map derived from MI data.